PCCP

Accepted Manuscript

ROYAL SOCIETY OF CHEMISTRY

www.rsc.org/pccp

Journal Name

RSCPublishing

ARTICLE

Optimal top electrodes for inverted polymer solar cells

Cite this: DOI: 10.1039/x0xx00000x

Hye Rim Yeom,‡ [a] Jungwoo Heo,‡ [b] Gi-Hwan Kim,[a] Seo-Jin Ko,[a] Seyeong Song,[a] Yimhyun Jo,[c] Dong Suk Kim,[c] Bright Walker*[a] Jin Young Kim* [a]

Received 00th January 2012,
Accepted 00th January 2012

DOI: 10.1039/x0xx00000x

www.rsc.org/

Although polymer solar cells (PSCs) have received a tremendous amount of attention in recent years, a number of criteria must be met in order for them to be suitable as practical and commercially feasible power sources, including high performance, good air stability and inexpensive manufacturing. In this contribution, we determine the optimal top electrode for practical PSC fabrication by investigating the influence of the electrode material on the optical properties and performance of PSC devices. The optical properties of eight metals were considered, out of which three metal electrodes (aluminum (Al), silver (Ag), gold (Au)) with the best optical properties were used to prepare inverted PSC devices comprising a blended polymer thieno[3,4-*b*]thiophene/benzodithiophene (PTB7) and [6,6]-phenyl C_{71}-butyric acid methyl ester ($PC_{71}BM$). Among the photovoltaic parameters, the short circuit current density (J_{SC}) was most strongly affected by the optical properties of the top electrode. In the results of experiment, the J_{SC} of the Al and Ag electrode devices were found to be approximately 13 % (15.1→13.1 mA cm^{-2}) higher than Au electrode device due to the significant parasitic absorption of light by Au at wavelengths below 600 nm. In contrast, Al and Ag electrodes have high reflectance throughout the visible spectrum, which leads to high J_{SC}. Ag electrodes have relatively good stability to ambient exposure, maintaining over 96 % of the original efficiency after 170 hours; this stability is comparable stability to Au. These data lead to the conclusion that Ag is the optimal top electrode material for use in inverted devices.

Introduction

Polymer solar cells (PSCs) based on thin film conjugated polymer/fullerene compounds have attracted attention due to their potential applications in light weight, low-cost, flexible, and large-area solution processed devices.[1-6] Recently, the power conversion efficiency of PSCs has reached 11 %, while 10 % has been estimated as the threshold efficiency for commercial applications.[7,8] For the commercialization of PSCs, stability and mass production techniques still require further development. Therefore, significant research efforts have recently focused on enhancement of PSC stability. Inverted polymer solar cells (iPSCs) offer distinct advantages for long term air stability compared to conventional polymer solar cells (cPSCs) by avoiding the corrosive and hygroscopic p-type buffer layer poly(3,4-ethylenedioxylenethiophene):poly (styrenesulphonicacid) (PEDOT:PSS) and easily oxidizable metal cathodes.[9,10] Inverted devices differ from conventional devices by using an n-type transparent substrate and high work function top electrode; many studies have been attempted to identify optimal materials and processing conditions to construct this architecture. Early work with iPSCs, explored the use of various n-type, p-type metal oxides to achieve symmetry breaking in iPSCs, such as titanium oxide (TiO_x), zinc oxide (ZnO) or molybdenum oxide (MoO_3), vanadium oxide (V_2O_5) have been introduced between the active layer and the electrodes.[11-13] However, there are inherent incompatibilities at the organic active layer/inorganic metal oxide interface. Therefore, recently, conjugated polyelectrolyte (CPE) have been introduced at the interface between the organic active layer and inorganic metal oxide in order to improve compatibility at the organic/inorganic interface.[14-16] Although TiO_x or ZnO layers have been demonstrated as effective n-type buffer layers, they can reduce the amount of light absorption within the active layer due to absorb in the blue to ultraviolet (UV) wavelength region.[17,18] To reduce this absorption loss, more transparent organic materials such as Polyethylenimine ethoxylated (PEIE), branched polyethylenimine (PEI) and poly[(9,9-bis(3′-(N,N-dimethylamino) propyl)-2,7-fluorene)-alt-2,7- (9,9-dioctylfluorene)] (PFN) have been introduced in iPSCs as n-type buffer layers instead of ZnO or TiO_x[19-21]

In this article, we focus on the identification of optimal top electrode materials for use in iPSCs. We explore various anode metals including aluminum (Al), silver (Ag), gold (Au), copper (Cu), palladium (Pd), platinum (Pt), nickel (Ni), and molybdenum (Mo) to identify relationships between the inherent optical properties of the top electrode and device performance. The reflectance of three top electrodes (Al, Ag, and Au) was studied using ultraviolet- visible (UV-Vis) spectroscopy in reflection mode, while electrode work functions were determined by ultraviolet photoelectron spectroscopy (UPS). Solar cell devices were fabricated in the inverted structure using a bulk heterojunction consisting of the conjugated polymer thieno[3,4-*b*]thiophene/ benzodithiophene (PTB7) and [6,6]-phenyl C_{71}-butyric acid methyl ester ($PC_{71}BM$) with different metal electrodes. The optical properties of these devices were simulated by transfer matrix modeling (TMM) and compared to the measured properties of the cells. Analysis of the simulations, experimental data and device stability lead to the unambiguous identification of Ag as the optimal anode for use in inverted devices, which is found to yield an efficiency of 8.19 % in PTB7-based iPSCs.

Results and discussion

Optical properties and device characteristics

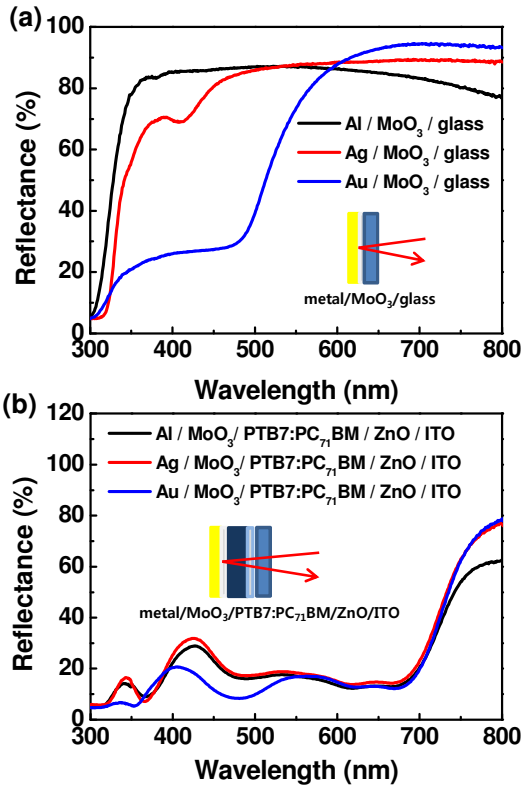

Figure 1. Comparison of reflectance of three types of metals (Al, Ag and Au) (a) deposited on glass/MoO_3 substrates films and (b) as completed solar cell devices (glass/ITO/PTB7:$PC_{71}BM$/MoO_3/metal).

Solar cell devices function by absorbing light in the active layer after it has passed through a transparent front electrode. Active layers in polymer solar cells are typically close to 100 nm thick, with relatively low optical densities, and transmit a large fraction of this incident light. Light which is not absorbed in the first pass may be reflected from a top metal electrode and pass through active layer again, allowing additional absorption to take place. As a result, the optical properties of top metal electrode strongly correlate with light harvesting in the active layer. Generally in iPSCs, one of three metals (Al or Ag or Au) is typically used as top electrode, with a high-work function layer of MoO_3 to facilitate the extraction of holes. To investigate the optical properties inherent to commonly used top electrodes, the reflectance of three metals (Al or Ag or Au) /MoO_3 films were measured. The MoO_3 film and metal film thickness were fixed at 3.7 nm and 100 nm, respectively. As shown in **Figure 1**a, three metal/MoO_3 films have considerably different reflectance spectra. The Au/MoO_3 film is much less reflective than Ag/MoO_3 or Al/MoO_3 at wavelengths below 600 nm wavelength, which corresponds to the Au overturn absorption peak. In contrast, the Ag/MoO_3 and Al/MoO_3 films have high reflectance throughout the visible spectrum, except wavelengths around 420 nm and over 600 nm, respectively. The reflectance curves of Ag/MoO_3 and Al/MoO_3 films are well matched with Ag and Al overturn absorption. Inverted structure devices were fabricated with three metal electrodes and compared the corresponding reflectance spectra. In completed solar cell devices, interference of incident light occurs within each layer, where incident light interacts with light reflected from the top electrode (see **Figure 1**b). Here, the Au electrode device has lower reflectance than Ag or Al electrodes at less than 600 nm wavelength while the Al electrode device has lower reflectance than Ag and Au at wavelengths above 600 nm. This indicates that throughout all of the layers in the device, the intensity of reflected light is largely determined by the reflectivity of the top electrode.

Figure 2a present the device structure (glass /ITO (150 nm) /ZnO (60 nm) /PTB7:$PC_{71}BM$ (80 nm) /MoO_3 (3.7 nm) /top electrode (100 nm)) and the morphology of three kinds of top electrodes. The details of device fabrication are included in the experimental section. Each type of metal has different material properties (such as density, and melting point) and grows by different mechanisms under thermal evaporation condidtions.[22-25] Additionally, the morphology of each type of metal may be affected by parameters such as evaporation rate or temperature. To investigate the effect of evaporation rate and morphology on device properties, 100 nm films of each type of electrode were prepared using different evaporation conditions; the morphology and conductivity of the anodes were characterized via scanning electron microscope (SEM) and Van der Pauw method, respectively, (See **Figure S1** and **Table S2**) for samples prepared using slow (0.2 Å/s) or fast (1.5 Å/s) evaporation rates. The Al electrodes show the strongest dependence on evaporation rate, exhibiting very large grain sizes (greater than 1 μm) when evaporated slowly and smoother, sub-micrometer features when evaporated quickly;

the conductivity of Al electrodes was found to be 1.7×10^5 $\Omega^{-1}cm^{-1}$ for slowly evaporated films and approximately doubled to 3.4×10^5 $\Omega^{-1}cm^{-1}$ when evaporated quickly, reflecting the different morphologies. These differences presumably result from the reaction of Al vapour with trace gasses present in the evaporation chamber when evaporated slowly. Ag and Au morphologies showed weaker dependence on evaporation rate, yielding slightly smoother films when evaporated quickly. The conductivities of Ag electrodes were 3.7 and 3.9×10^5 $\Omega^{-1}cm^{-1}$ for electrodes evaporated slowly or quickly, respectively, while the conductivities of Au electrodes were 3.1 and 3.0×10^5 $\Omega^{-1}cm^{-1}$ for electrodes evaporated slowly or quickly, respectively. In any case, the conductivities were found to be about two orders of magnitude greater than the conductivity of the ITO electrodes (5.2×10^3 $\Omega^{-1}cm^{-1}$) indicating that the current through the electrodes is limited by the ITO films and not the top electrodes.

Figure 2b compares the current density - voltage (*J-V*) characteristics of iPSCs with three types of top electrodes under AM 1.5G illumination. The photovoltaic parameters are summarized in **Table 1**. These values represent the averages of five devices. The power conversion efficiency (PCE) using Al electrodes is 7.14 ± 0.13 %, with a short-circuit current density (J_{SC}) of 14.6 ± 0.26 mA cm^{-2}, an open-circuit voltage (V_{OC}) of 0.75 ± 0.01 V and fill factor (*FF*) of 0.65 ± 0.01, while Ag electrodes yield a PCE of 8.00 ± 0.22 % (J_{SC} = 14.8 ± 0.39 mA cm^{-2}, V_{OC} = 0.75 ± 0.00 V and *FF* = 0.72 ± 0.01), and Au electrodes yield a PCE of 6.58 ± 0.41% (J_{SC} = 12.9 ± 0.62 mA cm^{-2}, V_{OC} = 0.75 ± 0.01 V and *FF* = 0.69 ± 0.01). Despite using metals with different work functions[26], the V_{OC} values are same (0.75 V) in all cases. Thin n-type and p-type buffer layers can be introduced between the active layer and the electrodes to modify the effective work functions of the electrodes and create Ohmic contacts. When Ohmic contacts are created, the V_{OC} depends only on the difference between the highest occupied molecular orbital (HOMO) level of the donor and the lowest unoccupied molecular orbital (LUMO) level of acceptor, rather than the difference of work function between the two electrodes.[27,28] UPS was carried out to confirm the work function of the three anodes with a thin MoO_3 layer (3.7 nm). The spectra show significant differences at high intensity, indicating that the metal underneath the thin MoO_3 affects the spectrum, however, all three samples exhibit the same shoulder feature at the secondary edge, indicating that the thin MoO_3 results in the same work function (5.2 eV) regardless of whether it is deposited on Al, Ag or Au. (**Figure. S2**). Thus, even though only 3.7 nm of MoO_3 is used, it is effective at shifting the work function of all 3 electrodes to the same value and creating an Ohmic anode contact.

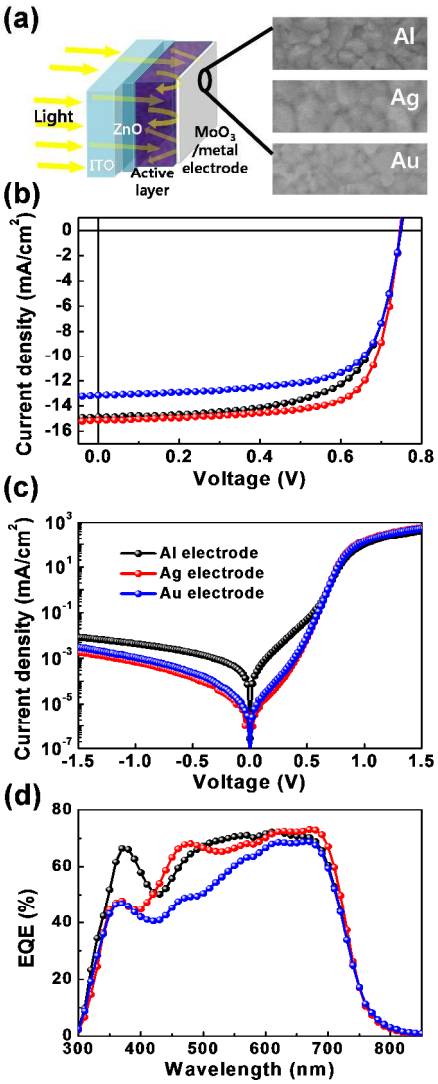

Figure 2. Device characteristics. (a) Schematic diagram showing device architecture with electrode morphologies (500 nm x 168 nm). (b) Comparison of *J-V* characteristics in PTB7: $PC_{71}BM$ inverted devices with aluminum (Al), silver (Ag), and gold (Au) top electrodes under illumination and (c) in dark condition. (d) External quantum efficiency (EQE) spectra corresponding to the same devices.

Journal Name

RSCPublishing

ARTICLE

Table 1. Photovoltaic parameters of PTB7: $PC_{71}BM$ inverted devices with different top electrodes.

Electrode	J_{SC} [mA cm^{-2}]	V_{OC} [V]	*FF*	PCE [%]	J_{SC} (calc.) [b] [mA cm^{-2}]	R_s [Ωcm^2]	R_{sh} [Ωcm^2]
Al [a] (n = 5)	14.6 ± 0.26 (14.9) [c]	0.75 ± 0.01 (0.75) [c]	0.65 ± 0.01 (0.66) [c]	7.14 ± 0.13 (7.35) [c]	15.1	6.00 ± 0.1	496 ± 7.9
Ag [a] (n = 5)	14.8 ± 0.39 (15.1) [c]	0.75 ± 0.00 (0.75) [c]	0.72 ± 0.01 (0.73) [c]	8.00 ± 0.22 (8.19) [c]	15.1	3.08 ± 0.1	753 ± 5.4
Au [a] (n =5)	12.9 ± 0.62 (13.5) [c]	0.75 ± 0.01 (0.75) [c]	0.69 ± 0.01 (0.70) [c]	6.58 ± 0.41 (6.93) [c]	13.4	4.92 ± 0.6	607 ± 3.3

[a] Device structure : ITO/ZnO/PTB7:$PC_{71}BM$/MoO_3/electrode. Here n represents the number of devices for averaging the final values (see Supporting Information Table S1). [b] J_{SC}(calc.), calculated J_{SC} from a EQE curve. [c] Best performance

Although the active layers, device structures and MoO_3 contacts were prepared using identical procedures, the *FF* exhibits considerable variation when the electrode metal is changed. The Ag electrode device reaches a peak *FF* of 72 % while the Au electrode shows a similar *FF* up to 69 %. The *FF* using the Al electrode, however, reaches only 65 %. Generally, the *FF* is related to shunt resistance (R_{sh}) and series resistance (R_S). Poor electrical contact leads to high R_S and decreased *FF*.[29,30] In case of Al electrodes, during the thermal evaporation of Al, chemical reactions may occur between MoO_3 and Al,[12] leading to by-products such as MoO_2 and Al_2O_3 which lower the *FF*.[31] For this reason, Al electrodes results in the highest R_S (**Table 1**). The dark curves for Ag and Au electrode devices show a larger rectification (up to 6 orders of magnitude in the range of ±1.5 V) and smaller reverse saturation currents than the Al electrode device (**Figure 2**c). This result indicates that Ag and Au electrodes devices result in lower charge recombination losses than the Al electrodes.

Figure 2d shows the external quantum efficiency (EQE) spectra of each device, which corresponds to their J_{SC}s. For each device, all processes (except for the top electrode material) were carried out under identical conditions; notably the blending condition and thickness (approximately 80 nm) are identical for each device. Nevertheless, the device with Au electrodes exhibits a lower J_{SC} (calc. J_{SC} = 13.4 mA cm^{-2}) compared to Ag (calc. J_{SC} = 15.1 mA cm^{-2}) and Al (calc. J_{SC} = 15.1 mAcm^{-2}, see **Table1**). Moreover, we show the interesting result that Al and Ag electrodes devices produce the same J_{SC} despite having different EQE curves. Because the devices are otherwise identical, it follows that these differences in EQE arise from differences in the reflectance of Al and Ag.

In order to thoroughly investigate the influence of optical properties on J_{SC}, we have compared the absorption difference ($\Delta\alpha$) between devices with Ag electrodes and Au electrodes, applying the equation in **Figure 3**a to the reflectance spectra in **Figure. 1**b. $\Delta\alpha$ is compared to the difference in EQE using Ag and Au electrodes in **Figure 3**b. Notably, the change in absorbance closely matches the change in EQE, indicating that the reflectivity of the top electrode directly influences light harvesting in the active layer. This tendency was seen in not only PTB7:$PC_{71}BM$ inverted solar cells but also P3HT:$PC_{61}BM$ inverted solar cells (see **Figure S3** and **Table S3**).

Optical modelling

In order to thoroughly explore how the optical properties of the top electrode influence photocurrent generation in iPSCs, a numerical simulation was carried out using, TMM.[32-34] Absorption not only by the active layer but also by the electrode was investigated via TMM. The distribution of the modulus squared of electric field intensity ($|E|^2$), which is directly proportional to the charge carrier generation in the active layer, was also considered.[32,33] Computational details are included in the supporting information (S.I). Simulated absorption by the active layer and the top electrodes are shown in **Figure 4**a. The device with Al electrodes shows the highest absorption in the active layer, while the Au electrode device displays significantly reduced absorption of light at wavelengths from 400 nm to 600 nm. This drop in active layer absorption coincides with a region of strong absorption by the Au electrode. The parasitic absorption of each electrode corresponds well with changes in the active layer absorption and explains the differences in the measured absorption spectra of the active layer with each electrode. Although Al absorbs a considerable amount of the light above 600 nm, absorption by PTB7 blends drops off rapidly above 700 nm and little difference is observed between the absorption spectra above 600 nm. The tendencies of the light absorption in the active layer modeled by TMM are consistent with changes observed in the shape of EQE spectrum of each device in **Figure 2**c.

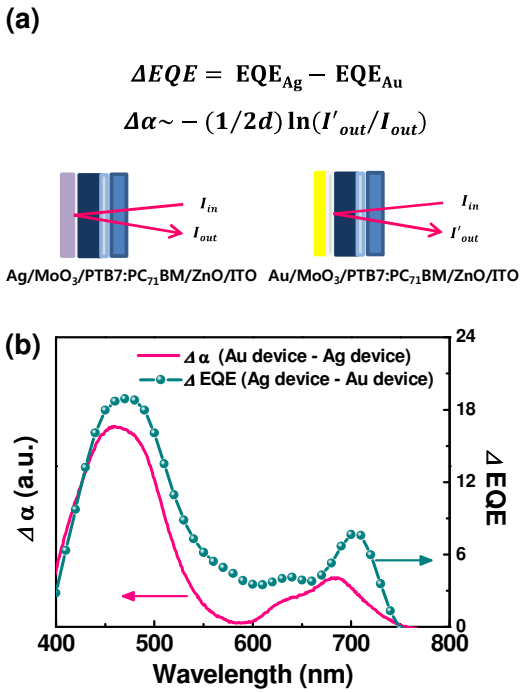

Figure 3. (a) Equations used to determine EQE difference (ΔEQE) and absorption difference (Δα) here, d is the PTB7:$PC_{71}BM$ film thickness (80 nm). I'_{out} is the intensity of the reflected light from the Au electrode device and I_{out} is the intensity of the reflected light from the Ag electrode device) as well as device schematics showing the optical beam path through the samples. (b) Comparison of Δα between the Au electrode device and the Ag electrode device (left y-axis) with ΔEQE ($EQE_{Ag} - EQE_{Au}$) (right y-axis).

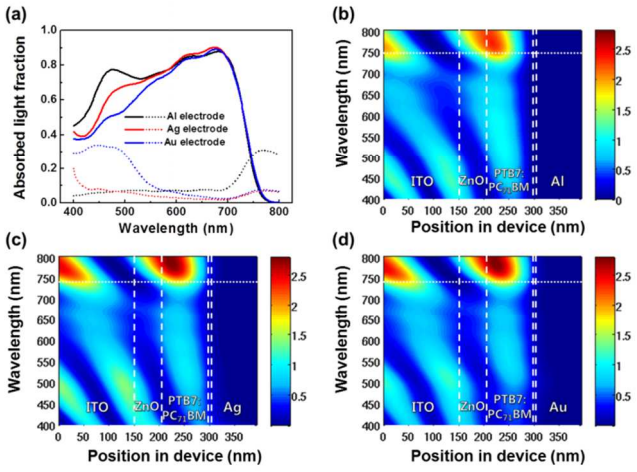

Figure 4. Simulated optical properties of PTB7:$PC_{71}BM$ inverted solar cells with different top electrodes. (a) Absorbed light fraction. Solid lines show the absorption in the active layer while dotted traces show the parasitic absorption of the top electrode. (b) - (d) Normalized electric field intensity. (b), (c), and (d) correspond to devices having Al, Ag, and Au electrodes, respectively. White dashed lines indicate the boundaries of each layer and white dotted traces represent absorption onset of PTB7:$PC_{71}BM$.

Figure 4(b-d) shows the distribution of the $|E|^2$ in each device with different electrodes. **Figure 4**b shows strong intensity in the visible region compared with **Figure 4**c and d, implying Al has superior reflectance within the visible range. Due to absorption in near IR region, $|E|^2$ is lower than the other metals at wavelengths of higher than 700 nm. Because the active layer absorbs little light at wavelengths greater than 700 nm, this parasitic absorption does not adversely affect photocurrent generation and it is apparent that Al is the best choice to maximize J_{SC} in terms of optical properties. In the case of Ag, a parasitic absorption of light at the wavelength below 470 nm results in reduced $|E|^2$ intensity compared to Al electrode device, as shown in **Figure 4**c. Nonetheless, due to the high reflectance of light at wavelengths greater than 470 nm, the simulated J_{SC} produced by the Ag electrode device is comparable to that of using Al. (16.8 mA cm^{-2} for the device with Al electrode and 16.2 mA cm^{-2} for that with Ag electrode). For active materials which absorb significant amounts of light at wavelengths greater than 700 nm, Ag electrodes may allow even higher J_{SC}s compared to Al electrodes. $|E|^2$ plots for Au electrodes are shown in **Figure 4**d, and exhibit relatively weak intensity up to 700 nm. This is due to the significant parasitic absorption by Au at wavelengths below 600 nm. This result demonstrates why devices with Au electrodes exhibit the lowest simulated J_{SC} (15.3 mA cm^{-2}) among the devices. In order to ascertain if these results apply to systems other than the PTB7:$PC_{71}BM$ system, the optical simulations and analysis were carried out for the P3HT:$PC_{61}BM$ system as well. Similar tendencies were observed from the simulated optical properties of P3HT:$PC_{61}BM$ inverted PSCs by TMM (**Fig. S4**). These data and simulations are consistent with the experimental results showing that Ag and Al top electrodes are advantageous for achieving optimal current density due to their high reflectance and low parasitic absorption compared to Au.

Other metals

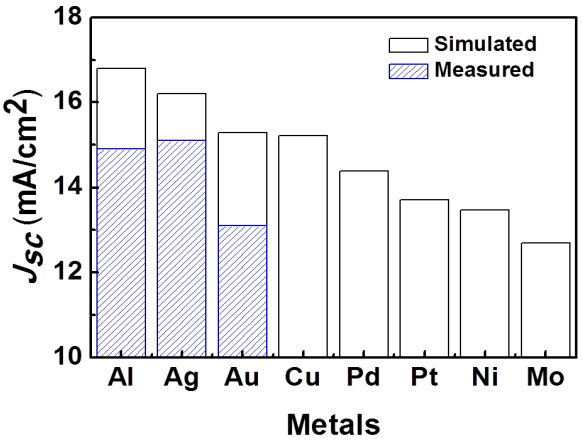

Figure 5. Simulated and measured Jsc in the PTB7:$PC_{71}BM$ inverted solar cells with each top electrode. IQE of the devices is assumed to be 100 %.

Table 2. Simulated J_{SC} of PTB7:$PC_{71}BM$ inverted solar cells with each top electrode and simulated absorbance of each metal electrode in the devices at wavelength of 400, 600, and 800 nm.

Metal (Φ, eV)	Simulated J_{SC} (mA cm^{-2})	Absorption fraction of each metal (%)		
		400 nm (Short λ)	600 nm (Middle λ)	800 nm (Long λ)
Al (4.3 eV)	16.8	4.08	7.1	28.7
Ag (4.7 eV)	16.2	19.9	2.9	6.2
Au (5.1 eV)	15.29	29.4	5.9	6.6
Cu (4.7 eV)	15.22	22.9	9.3	9.2
Pd (5.1 eV)	14.39	18.5	20.4	48.5
Pt (5.7 eV)	13.71	22.4	24.8	57.7
Ni (5.2 eV)	13.47	25.4	25	61.5
Mo (4.6 eV)	12.69	24.7	32.6	76.6

Although Al, Ag, and Au, are the most commonly used electrodes in inverted PSCs, it is possible to use other metals as top electrodes as well; we sought to carry out a comprehensive investigation of how a wider variety of metals affects the optical properties of OPV devices via TMM. Metals were selected which have appropriate work functions for use in the inverted structure and / or which have been applied as electrodes in other types of solar cells[35-37] including Copper (Cu), Palladium (Pd), Platinum (Pt), Nickel (Ni), and Molybdenum (Mo).

The J_{SC} of PTB7:$PC_{71}BM$ inverted solar cells was simulated using each type of anode. For the calculation of J_{SC}, the internal quantum efficiency (IQE) over all wavelengths was assumed to be 100 % implying that all photons absorbed in the active layer lead to photo-generated charge carriers which are extracted without any losses. Simulated J_{SC}s for devices using each anode metal are compared in **Figure 5**. Al, Ag, and Au are included for comparison. In order to further quantify differences in each metal, we simulated the fraction of light absorbed by the metal electrode inside the device at three discrete wavelengths (400, 600, and 800 nm representing short, mid, and long wavelength regions of the visible spectrum, respectively). These results are summarized in **Table 2**. Spatial distribution of modulus squared electric field inside the device for each metal electrode was also considered in **Figure S5**.

It is noteworthy that the Cu anode exhibits comparable J_{SC} to that of the device with the Au anode. Other metals, however, showed much lower J_{SC}. The Cu electrode absorbed 22.9 % of the incident light at 400 nm, and 9.3 % and 9.2 % at 600 and 800 nm respectively. The absorption was smaller at 400 nm and higher at 600 and 800 nm than those of Au (29.4 %, 5.9 %, and 6.6 % at 400, 600 and 800 nm, respectively.). Strong absorption at short wavelengths for both Cu and Au causes devices with these metal electrodes to generate relatively low J_{SC}s compared to Al and Ag.

Pd, Pt, Ni, and Mo electrodes all exhibited significant absorption across the visible spectrum and much higher absorption at 800 nm. Simulated JSCs for devices with Pd, Pt, Ni, and Mo electrodes were consistent with simulated absorption of each metal in the device. Although Mo is the most commonly used anode in thin film solar cells such as $Cu(In,Ga)Se_2$ cells, this metal absorbs the largest amount of light and is expected to result in a 25% reduction in current relative to Al when used in inverted polymer solar cells.

From these results, it is apparent that the optical properties of metal electrodes play a critical role in determining device properties of inverted PSCs. Unlike their thicker, inorganic counterparts, polymer solar cells cannot fully absorb the incident, non-reflected light in one pass, due to the thin active layers used in PSCs.[38] Therefore, the reflectivity of the metal electrode is a crucial contributor to the generation of current in PSC devices and it is clear that Al and Ag are the best choices for high reflectivity.

Air stability

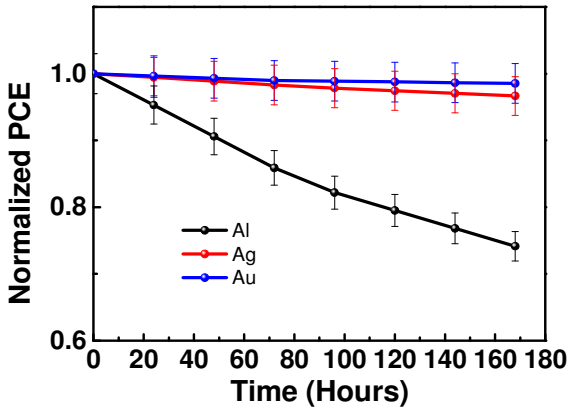

Figure 6. Normalized PCEs for PTB7:$PC_{71}BM$ inverted solar cells with different top electrodes as a function of storage time in air under ambient conditions without encapsulation.

In spite of the clear advantages offered by the optical properties of Al and Ag electrodes, Au electrodes have been more generally used in iPSCs. This may be because Au possesses excellent air stability due to its high work function. Therefore, we sought to compare the air stability of Al and Ag electrodes with Au. **Figure 6** shows the air stability of iPSCs in PTB7:$PC_{71}BM$ with three types of electrodes. Solar cells were exposed to air at room temperature without any encapsulation over a period of about 170 hours. After 170 hours, Au electrode devices maintained almost their original efficiency as expected. The Ag electrode devices performed similarly, retaining over 96 % of their original efficiency. The devices with Al electrodes, however, were significantly degraded to approximately 25 % of their original performance. These results show that the poor air stability of Al electrodes may limit the practical utility of this electrode even though this it offers good reflectivity and high J_{SC}.

Conclusions

In summary, we have elucidated relationships between the optical properties of top electrodes and the performance of inverted

architecture solar cells using a suite of different metals. The reflectivity of each metal electrode is found to considerably influence the light harvesting within the active layer. The three metals Al, Ag and Au are found to offer the best optical properties and yield the highest J_{SC}s via optimal utilization of reflected light. Among these three electrodes, Au suffers from the greatest parasitic absorption and the exhibits the lowest reflectance in the visible region, leading to significantly lower J_{SC}s compared to the other electrodes. Al and Ag electrodes, however, have relatively good reflectance across the visible spectrum and produce larger J_{SC}s. Al electrodes were found to lead to unstable devices with low *FF*s due to the low work function and reactivity of Al. These data, coupled with the advantage that Ag electrodes can be processed by solution methods such as printing or coating[39] lead to the conclusion that the optimal top electrode for use in iPSCs is Ag, offering high performance, good air stability and convenient processability. This study provides guidelines and rational for the selection of appropriate top electrodes in future PSC devices.

Experimental Section

Device fabrication and characterization

Inverted polymer solar cell devices were fabricated using the following procedure. First, ITO coated glass substrates were cleaned with detergent, then ultrasonicated in distilled water, acetone and isopropyl alcohol, then dried overnight in an oven at 100 ^{o}C. The ZnO layer was next deposited by diluting a diethylzinc solution (Aldrich, 15 wt.% in toluene) with two parts tetrahydrofuran[40] (note: the un-diluted diethyl zinc solution is highly reactive towards air and should be handled inside a glove box; after dilution with THF, the solution becomes less reactive, however, appropriate safety precautions should be taken in case of an accidental spill or fire), filtering through a 0.45 μm PTFE syringe filter and spin coating at 3000 rpm for 30 s in air. The ZnO layer was then annealed in air on a hot plate at 110 °C for 10 minutes, a ZnO film thickness was approximately 60 nm. Subsequently, substrates were transferred into a nitrogen filled glove box for spin-coating the active layer. A mixed solution of PTB7: $PC_{71}BM$ in chlorobenzene (concentration of 10 mg mL^{-1}) with 3 % DIO additive was then spin coated at 1300 rpm for 60 s on top of the ZnO layer to obtain a BHJ film with thickness of approximately 80 nm. Samples were then brought under vacuum (10^{-6} - 10^{-7} Torr), and MoO_3 (Thickness : ≈ 3.7 nm, evaporation rate : 0.1 Å/s) and Al (Thickness : ≈ 100 nm, evaporation rate : 1.5 Å/s) or Ag (Thickness : ≈ 100 nm, evaporation rate : 1.5 Å/s) or Au (Thickness : ≈ 100 nm, evaporation rate : 0.2 Å/s) metal electrodes were deposited on top of the BHJ layer by thermal evaporation with an area of 0.13 cm^2 for each device. Inverted devices using P3HT:$PC_{61}BM$ in *o*-dichlorobenzene (*o*-DCB) were prepared following the same procedure with concentration of 26 mg mL^{-1} and thickness of approximately 200 nm.

Current density-voltage measurements were collected using a Keithley 2635 source measure unit. Each device was scanned from -0.5 V to 1.0 V in 20 mV steps with a 50 ms integration time for each data point. J-V characterization was carried out inside a nitrogen filled glove-box using a high quality optical fiber to guide the light from a xenon arc lamp to the solar cell device. Each device had an active area of 13 mm^2, defined by an aperture placed over each device. Solar cell devices were illuminated with an intensity of 100 mW cm^{-2} as calibrated using a standard silicon reference cell (PV Measurements, Inc.) which had been standardized and certified at the National Renewable Energy Laboratory in Golden, Colorado. Error bars presented in stability data correspond relative errors of one standard deviation for current density-voltage measurements. EQE measurements were carried out using a QEX7 system manufactured by PV Measurements, Inc. UV-Vis reflectance spectra were measured on a Varian Cary 5000 spectrophotometer and UPS measurements were carried out using a KRATOS AXIS Nova instrument following previously reported procedures.[41] He I hv = 21.22 eV was used as a light source and thermally evaporated Au substrates were used as a reference. Work functions (Φ) were calculated from the onset of the secondary edge (E_{SE}) using the equation $\Phi = 21.22 - E_{SE}$.

Optical modelling by transfer matrix method

The transfer matrix method was utilized to calculate the absorption and $|E|^2$ intensity in each layer.[32-34] The film thickness of each layer was determined by examining cross-sectional samples via scanning electron microscopy (cross-sectional SEM). Measured thicknesses were: 150 nm for ITO, 60 nm for ZnO, 80 nm for PTB7:$PC_{71}BM$ blend, 200 nm for P3HT:$PC_{61}BM$ blend, 3.7 nm for MoO3, and 100 nm for top metal electrode. Thickness measurements were repeated several times and average values were taken.

In order to conduct the transfer matrix method, the complex number of refractive indices ($\tilde{n} = n + ik$), which are the function of wavelength ($\tilde{n}(\lambda)$), are needed for each layer. To get the extinction coefficient, *k*, the absorption spectrum of each layer was measured by UV-vis absorption spectroscopy followed by conversion into *k* by following relationship.

$$\frac{A}{l}\ln 10 = \frac{4\pi k}{\lambda}$$

where A stands for measured absorbance at the specific wavelength, l for the thickness of the film, and λ for the wavelength. The films were coated on the quartz substrate and the thickness of the film was measured by alpha step.

Since real and imaginary parts of complex refractive index satisfy Kramers-Kronig relation (K-K relation), which ensures two parts are inter-convertible each other, refractive index of active layer was derived from the calculated extinction coefficient using Hilbert function implemented in MATLAB. In order to validate that this calculation is applicable to our consideration, calculated refractive index was compared with other published data[42, 43] (**Fig. S6**). The calculated optical constants exhibit extrema at the same position and follow

previously reported spectra, confirming that the Kramers-Kronig transformation yields suitable refractive index data.

Acknowledgements

This research was supported by the BK21 Plus Program (META-material-based Energy Harvest and Storage Technologies, 10Z20130011057) funded by the Ministry of Education (MOE, Korea), the National Research Foundation of Korea Grant (NRF-2013R1A2A2A01015342, NRF-2013R1A1A2011591) and Development Program of the Korea Institute of Energy Research (KIER) (B4-2424).

Notes and references

[a] School of Energy and Chemical Engineering, Ulsan National Institute of Science and Technology (UNIST), Ulsan 698-798, South Korea. E-mail: jykim@unist.ac.kr, brightium@unist.ac.kr
[b] Department of Physics , Ulsan National Institute of Science and Technology (UNIST), Ulsan 698-798, South Korea.
[c] KIER-UNIST Advanced Center for Energy, Korea Institute of Energy Research, Ulsan 689-798, South Korea

† Electronic Supplementary Information (ESI) available: UPS spectra of each MoO_3/metal electrodes. *J-V* characteristics and simulated optical properties of P3HT:PC_{61}BM inverted devices. Simulated optical properties of PTB7:PC_{71}BM inverted solar cells with various metal electrodes (Cu, Pd, Pt, Ni and Mo). Complex reflective index of PTB7:PC_{71}BM blends. See DOI: 10.1039/b000000x/

‡ The first two authors contributed equally.

1. T. Erb, U. Zhokhavets, G. Gobsch, S. Raleva, B. Stühn, P. Schilinsky, C. Waldauf and C. J. Brabec, *Adv. Funct. Mater.*, 2005, **15**, 1193-1196.
2. G. Dennler, M. C. Scharber and C. J. Brabec, *Adv. Mater.*, 2009, **21**, 1323-1338.
3. Y. Kim, H. R. Yeom, J. Y. Kim and C. Yang, *Energy Environ. Sci.*, 2013, **6**, 1909-1916.
4. M. Kaltenbrunner, M. S. White, E. D. Głowacki, T. Sekitani, T. Someya, N. S. Sariciftci and S. Bauer, *Nat. Commun.*, 2012, **3**, 770.
5. S. H. Park, A. Roy, S. Beaupré, S. Cho, N. Coates, J. S. Moon, D. Moses, M. Leclerc, K. Lee and A. J. Heeger, *Nat. Photonics*, 2009, **3**, 297-303.
6. G. Yu, J. Gao, J. C. Hummelen, F. Wudl and A. J. Heeger, *Science*, 1995, **270**, 1789-1791.
7. NREL, Best research-cell efficiencies http://www.nrel.gov/ncpv/images/efficiency_chart.jpg, Accessed May, 2014.
8. R. F. Service, *Science*, 2011, **332**, 293.
9. Y. Sun, J. H. Seo, C. J. Takacs, J. Seifter and A. J. Heeger, *Adv. Mater.*, 2011, **23**, 1679-1683.
10. K. Norrman, M. V. Madsen, S. A. Gevorgyan and F. C. Krebs, *J. Am. Chem. Soc.*, 2010, **132**, 16883-16892.
11. G. Li, C.-W. Chu, V. Shrotriya, J. Huang and Y. Yang, *Appl. Phys. Lett.*, 2006, **88**, 253503.
12. C. Tao, S. Ruan, X. Zhang, G. Xie, L. Shen, X. Kong, W. Dong, C. Liu and W. Chen, *Appl. Phys. Lett.*, 2008, **93**, 193307.
13. C. Waldauf, M. Morana, P. Denk, P. Schilinsky, K. Coakley, S. A. Choulis and C. J. Brabec, *Appl.* Phys. *Lett.*, 2006, **89**, 233517.
14. H. Choi, J. S. Park, E. Jeong, G.-H. Kim, B. R. Lee, S. O. Kim, M. H. Song, H. Y. Woo and J. Y. Kim, *Adv. Mater.*, 2011, **23**, 2759-2763.
15. Y.-M. Chang and C.-Y. Leu, *J. Mater Chem A*, 2013, **1**, 6446-6451.
16. J. H. Seo, A. Gutacker, Y. Sun, H. Wu, F. Huang, Y. Cao, U. Scherf, A. J. Heeger and G. C. Bazan, *J. Am. Chem. Soc.*, 2011, **133**, 8416-8419.
17. H. Yang, S. Zhu and N. Pan, *J. Appl. Polym. Sci.*, 2004, **92**, 3201-3210.
18. Y. Jiang, R. Wilson, A. Hochbaum and J. Carter, Novel pigment approaches in optically variable security inks including polarizing cholesteric liquid crystal (CLC) polymers, San Jose CA **2002**.
19. A. K. K. Kyaw, D. H. Wang, V. Gupta, J. Zhang, S. Chand, G. C. Bazan and A. J. Heeger, *Adv. Mater.*, 2013, **25**, 2397-2402.
20. Z. He, C. Zhong, S. Su, M. Xu, H. Wu and Y. Cao, *Nat. Photonics*, 2012, **6**, 591-595.
21. Y. Zhou, C. Fuentes-Hernandez, J. Shim, J. Meyer, A. J. Giordano, H. Li, P. Winget, T. Papadopoulos, H. Cheun, J. Kim, M. Fenoll, A. Dindar, W. Haske, E. Najafabadi, T. M. Khan, H. Sojoudi, S. Barlow, S. Graham, J.-L. Brédas, S. R. Marder, A. Kahn and B. Kippelen, *Science*, 2012, **336**, 327-332.
22. G. Kaune, E. Metwalli, R. Meier, V. Körstgens, K. Schlage, S. Couet, R. Röhlsberger, S. V. Roth and P. Müller-Buschbaum, *ACS Appl. Mater. Interfaces*, 2011, **3**, 1055-1062.
23. G. Kaune, M. A. Ruderer, E. Metwalli, W. Wang, S. Couet, K. Schlage, R. Röhlsberger, S. V. Roth and P. Müller-Buschbaum, *ACS Appl. Mater. Interfaces*, 2008, **1**, 353-360.
24. G. Santoro, S. Yu, M. Schwartzkopf, P. Zhang, S. Koyiloth Vayalil, J. F. H. Risch, M. A. Rübhausen, M. Hernández, C. Domingo and S. V. Roth, *Appl. Phys. Lett.*, 2014, **104**, 243107.
25. C. W. Hollars and R. C. Dunn, *Review of Scientific Instruments*, 1998, **69**, 1747-1752.
26. M. Uda, A. Nakamura, T. Yamamoto and Y. Fujimoto, *J. Electron Spectrosc. Relat. Phenom.*, 1998, **88–91**, 643-648.
27. L.-M. Chen, Z. Hong, G. Li and Y. Yang, *Adv. Mater.*, 2009, **21**, 1434-1449.
28. J. H. Seo, H. Kim and S. Cho, *Phys. Chem. Chem. Phys.*, 2012, **14**, 4062-4065.
29. D. L. Meier and D. K. Schroder, Electron *Devices, IEEE Transactions on*, 1984, **31**, 647-653.
30. C. M. Proctor, M. Kuik and T.-Q. Nguyen, *Prog. Polym. Sci.*, 2013, **38**, 1941-1960.
31. S. M. Umbrajkar, M. Schoenitz and E. L. Dreizin, *Propellants, Explos., Pyrotech.*, 2006, **31**, 382-389.
32. G. F. Burkhard, E. T. Hoke and M. D. McGehee, *Adv. Mater.*, 2010, **22**, 3293-3297.
33. L. A. A. Pettersson, L. S. Roman and O. Inganäs, *J. Appl. Phys.*, 1999, **86**, 487-496.
34. P. Peumans, A. Yakimov and S. R. Forrest, *J. Appl. Phys.*, 2003, **93**, 3693-3723.
35. J. Kim, J. Kang, U. Jeong, H. Kim and H. Lee, *ACS Appl. Mater. Interfaces*, 2013, **5**, 3176-3181.
36. P.-C. Hsu, D. Kong, S. Wang, H. Wang, A. J. Welch, H. Wu and Y. Cui, *J. Am. Chem. Soc.*, 2014, **136**, 10593-10596.
37. T. Ishii, K. Otani, T. Takashima and K. Ikeda, *Progress in Photovoltaics: Research and* Applications, 2014, **22**, 949-957.

38. J. H. Yim, S.-y. Joe, C. Pang, K. M. Lee, H. Jeong, J.-Y. Park, Y. H. Ahn, J. C. de Mello and S. Lee, *ACS Nano*, 2014, **8**, 2857-2863.
39. F. C. Krebs, *Sol. Energy Mater. Sol. Cells*, 2009, **93**, 394-412.
40. W. J. E. Beek, L. H. Slooff, M. M. Wienk, J. M. Kroon and R. A. J. Janssen, *Adv. Funct. Mater.*, 2005, **15**, 1703-1707.
41. J. H. Seo, R. Yang, J. Z. Brzezinski, B. Walker, G. C. Bazan and T.-Q. Nguyen, *Adv. Mater.*, 2009, **21**, 1006-1011.
42. J. You, X. Li, F.-x. Xie, W. E. I. Sha, J. H. W. Kwong, G. Li, W. C. H. Choy and Y. Yang, *Adv. Energy Mater.*, 2012, **2**, 1203-1207.
43. G. J. Hedley, A. J. Ward, A. Alekseev, C. T. Howells, E. R. Martins, L. A. Serrano, G. Cooke, A. Ruseckas and I. D. W. Samuel, *Nat Commun*, 2013, **4**, 2867.

Graphical Abstract

Optimal top electrodes for inverted polymer solar cells

Hye Rim Yeom, Jungwoo Heo, Gi-Hwan Kim, Seo-Jin Ko, Seyeong Song, Yimhyun Jo, Dong Suk Kim, Bright Walker, Jin Young Kim

Textual Abstract

A variety of metals were investigated as electrodes in inverted organic solar cell devices; highly reflective silver electrodes were found to yield outstanding performance and stability compared to other metals.

ToC figure